© 2024 IEEE. Personal use of this material is permitted. Permission from IEEE must be obtained for all other uses, in any current or future media, including reprinting/republishing this material for advertising or promotional purposes,creating new collective works, for resale or redistribution to servers or lists, or reuse of any copyrighted component of this work in other works. https://dx.doi.org/10.1109/IGARSS53475.2024.10641721

A METHOD FOR CORRECTING THE GPS NAVIGATION BIT TRANSITIONS IN THE FY-GNOS-II GNSS-R PAYLOAD

C. Wang[1,2], K. Yu[1], H. Park[2,3], A. Camps[2,3,4]

[1]School of Environment and Spatial Informatics, China University of Mining and Technology, Xuzhou, Jiangsu, China
[2]CommSensLab – UPC, Universitat Politècnica de Catalunya – BarcelonaTech, Barcelona, Spain
[3]Institut d'Estudis Espacials de Catalunya (IEEC) – CTE-UPC, E-08034 Barcelona, Spain
[4]ASPIRE Visiting International Professor, UAE University, CoE, POBox 15551 Al-Ain, UAE

ABSTRACT

Global Navigation Satellite System Reflectometry (GNSS-R) is a remote sensing technology that uses GNSS signals reflected over Earth's surface, offering advantages such as high spatio-temporal resolution and cost-effectiveness. GPS navigation signals convey navigation information through the navigation bits, in which phase jumps occur randomly at 20 ms interval. However, navigation information is meaningless in GNSS-R and limits the coherent integration time. This study presents a technique to mitigate the impact of the navigation bits on the generation of DDMs by using the raw GNSS-R data from the Fengyun-3E (FY-3E) satellite. Sample results show that, after correcting for the navigation bits, the signal-to-noise ratio (SNR [dB]) of DDMs increased by ~0.4 dB over sea to up to 3 dB over sea ice, showing that this improvement is very significant for coherent targets. The proposed navigation bit correcting method in this study significantly improves the usability of these DDMs, and opens the door to other applications that require larger integration times.

Index Terms—Spaceborne GNSS-R, navigation bit, SNR, FY-3E.

1. INTRODUCTION

Spaceborne GNSS-R is currently a hotspot in the field of remote sensing. Most commonly used GNSS-R satellites include UK TechDemoSat-1 satellite (TDS-1), and NASA Cyclone GNSS (CYGNSS) microsatellites. Numerous investigations rely on the substantial volume of data generated by these satellites, in various domains such as sea surface wind retrieval (e.g. [1]), significant wave height retrieval (e.g. [2]), sea ice detection (e.g. [3]), soil moisture retrieval (e.g. [4]), and flood detection (e.g. [5]). China's FY-3E satellite was launched on July 5th, 2021. It is the world's first civil dawn/dusk orbit weather satellite providing supplement the global atmospheric sounding information during the dawn/dusk period [6]. This satellite carries the Global Navigation Satellite System Occultation Sounder II (GNOS II) payload, which can perform stable and high-precision GNSS-RO (GNSS-Radio Occultations) and GNSS-R observations.

In the GPS system, the navigation bit produces π radians phase jumps randomly occurring with a period of 20 ms. During the generation of DDMs from GNSS-R raw data, if the coherent integration time exceeds 1 ms (e.g., 2 ms, 3 ms), navigation bit transitions may lead to a phase reversal during the coherent integration [7], resulting in decrease in the DDM peak, SNR. Based on ground-based experiments, Valencia et al. [8] previously employed an algorithm based on thresholding the first derivative of the phase to correct the navigation bit effect and achieved favorable results. However, for spaceborne GNSS-R technology, the position of the signal specular reflection points changes every 1 ms, and there is a higher impact from the reflection signal environment. Therefore, it is difficult to detect the transitions of the navigation bit. To address this issue, this study proposes an effective method to eliminate navigation bit transitions. As a result, that significantly improves the SNR when generating DDMs using FY-3E raw data.

2. THE IMPACT OF NAVIGATION BIT ON DDM

The GNSS-R observable used in this study is the Delay Doppler Map (DDM) obtained by cross-correlation the locally-generated GPS C/A codes and reflected signals on the earth surface acquired from the FY-3E GNOS II payload.
In this study, the resulting individual DDM (i.e., before incoherent averaging) is a 3000×20 matrix with ~0.06 chip and 400 Hz resolutions, respectively:

$$DDM(t_m,\tau,f_D) = \int_0^{T_c} r(t+t_m)CA(t+\tau)exp(-j2\pi\cdot f_D\cdot t)dt \quad (1)$$

where $DDM(\tau, f_D)$ denotes the DDM raw count at a delay of τ and a Doppler frequency of f_D from the specular point; $r(t)$ is reflect signal, $CA(t)$ is GPS C/A code's local replica and T_c is coherent integration time. Moreover, in practical applications of spaceborne GNSS-R missions, the DDM calculated from 1 ms data is highly susceptible to speckle noise. Therefore, it is necessary to perform incoherent Eq. (2) or coherent Eq. (3) accumulation of multiple adjacent individual DDMs to mitigate the effects of noise [9]:

$$\langle \left|DDM_{multi}^{incoh}(\tau,f)\right|^2 \rangle = \frac{1}{N}\sum_{m=1}^{N}|DDM(t_m,\tau,f)|^2 \qquad (2)$$

$$\langle \left|DDM_{multi}^{coh}(\tau,f)\right|^2 \rangle = \left|\frac{1}{N}\sum_{n=1}^{N}DDM(t_n,\tau,f)\right|^2 \qquad (3)$$

where $DDM(t_m,\tau,f)$ is given by Eq. (1), $t_m = m \cdot T_c$. $DDM_{multi}(\tau,f)$ is the result obtained by accumulating individual DDMs. Besides, the SNR is calculated as follows [2]:

$$SNR(\mathrm{dB}) = 10 \times \log_{10}\left(\frac{S_{max}}{N_f}\right) \qquad (4)$$

where S_{max} denotes the maximum value of the DDM raw counts, and N_f is the noise floor outside of the DDM.

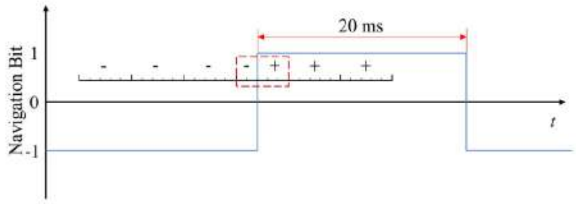

Fig. 1. Schematic representation of navigation bit change. The blue line represents navigation bits, and the black line represents a segment of 30 ms reflected signal with a coherent integration time of 5 ms and 6 incoherent integrations.

Figure 1 illustrates an example of the transitions of the navigation bits, causing changes in the signal polarity every 20 ms (but not necessarily every 20 ms). When T_c in Eq. (1) equals 1 ms, navigation bits do not significantly affect the computation of the DDM_{multi} (because at most, it will effect only 1 out of 20 individual DDMs). However, when T_c is larger than 1 ms (e.g., 2 ms, 3 ms), the change to have phase jumps in the reflected signal are higher, as illustrated by the red dashed box in Fig. 1. This situation can impact the computation of DDM_{multi}.

3. NAVIGATION BIT CORRECTION

This study proposes a method to address the issue above, which involves multiplying all individual 1 ms DDMs by a compensation vector, denoted as $Sign$, before computing Eq. (2) or Eq. (3). This is a one-dimensional vector composed solely of 1's and -1's. First, individual DDMs is grouped together up to of T_s, where T_s is search window an integer not exceeding 40 ms (2 navigation bits). So for each group, there will only be 0, 1 or 2 navigation bit transitions. As shown in Fig. 2, there are 3 cases of $Sign$. As shown in Eq. (2) and Eq. (3), DDM_{multi} is obtained by summing the absolute values of the individual DDMs. Therefore, in Case 2 of Fig. 2 (where each group contains only one navigation bit transition), the same DDM_{multi} will be obtained if the 1st to t_{s2}th bits of the $Sign$ vector are 1's while the rest of the bits are -1's, or if the 1st to t_{s2}th bits of the $Sign$ vector are -1's while the rest of the bits are 1's. The same applies to Case 1 and Case 3. Therefore, Case 2 has $T_s - 1$ combinations while Case 1 only has 1 combination and Case 3 has $T_s - 21$ combinations. Besides, T_s should be divisible by T_c to ensure complete rounds of coherent summation within each group. For instance, when T_c=2 ms, T_s=40 ms; when T_c= 3 ms, T_s=39 ms.

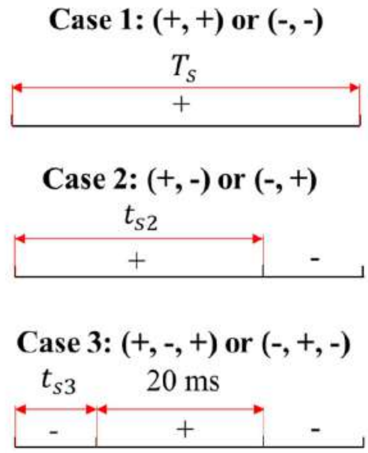

Fig. 2. Methods to determine the values of the elements of the $Sign$ vector. t_{s2} and t_{s3} are integers in ms. In the second case, $t_{s2} \in [1\ \mathrm{ms}, T_s - 1\ \mathrm{ms}]$; in the third case, $t_{s3} \in [1\ \mathrm{ms}, T_s - 21\ \mathrm{ms}]$.

Above all, there are $2T_s$-21 (≤ 59) combinations for the $Sign$ vector. Due to the consideration of nearly 40 individual DDMs each time when selecting the $Sign$ vector, this method effectively mitigates the impact of speckle noise in the DDMs, which allows the DDM's shape to pop up above the noise in T_s ms. The equation to calculate $DDM_{multi}(\tau,f)$ composed of T_s individual DDMs is given by:

$$\langle |DDM_{multi}(\tau,f)|^2 \rangle = \frac{1}{M_{incoh}N_{coh}} \cdot \sum_{m=1}^{M_{incoh}}\left|\sum_{n=1}^{N_{coh}} DDM(t_{mn},\tau,f)\cdot Sign(t_{mn})\right|^2 \qquad (5)$$

where M_{incoh} is the incoherent integrations, and N_{coh} is coherent integration time. Depending on the sign vectors, $2T_s$ -21 DDM_{multi} 's are obtained, among which the DDM_{multi} with the highest SNR is considered the final DDM_{multi}. This method involves a significant computational load. If T_s exceeds 40 ms (more than 2 navigation bits), it would result in a greater number of $Sign$ combinations, further substantially increasing the computational load.

4. EXPERIMENT AND RESULT

This study selected the Spitsbergen region (approximately 78.9 N; 11.9 E) as the research target. The terrain in this area is complex, featuring a diverse range of reflecting surfaces, including ocean surfaces, sea ice, soil, snow-covered ground, and mountainous terrain. Therefore, the data generated in this region are well-suited for studying GNSS-R sensitivity to the roughness of different reflecting surfaces. Data from three reflecting surfaces were chosen, including sea water surface data (May 6_{th}, 2022, at 13:34h); sea ice surface data (February 24_{th}, 2022, at 12:41h); and soil surface data (August 15_{th}, 2022, at 8:17h).

As shown in Fig. 3, points of three different colors represent the trajectories of FY-3E's specular points in 1.5 seconds during the three selected times. Figure 4 presents the DDM images of sea ice surface, when T_c (coherent integration time) is 2 ms and M_{incoh} (the number of incoherent integrations) is 500. From Fig. 4, it is evident that navigation bit correction effectively removes noise from the DDMs and increased the SNR. Table 1 presents the uncorrected DDM SNR, and the corrected SNR under different N_{coh} and M_{incoh}. In Table 1,

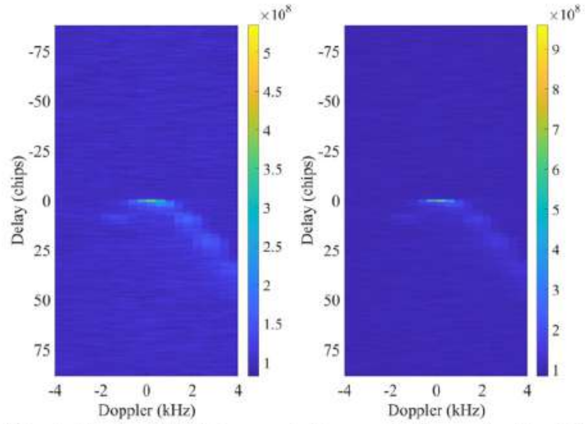

Fig. 4. Sea ice DDM images before, and after navigation bit correction.

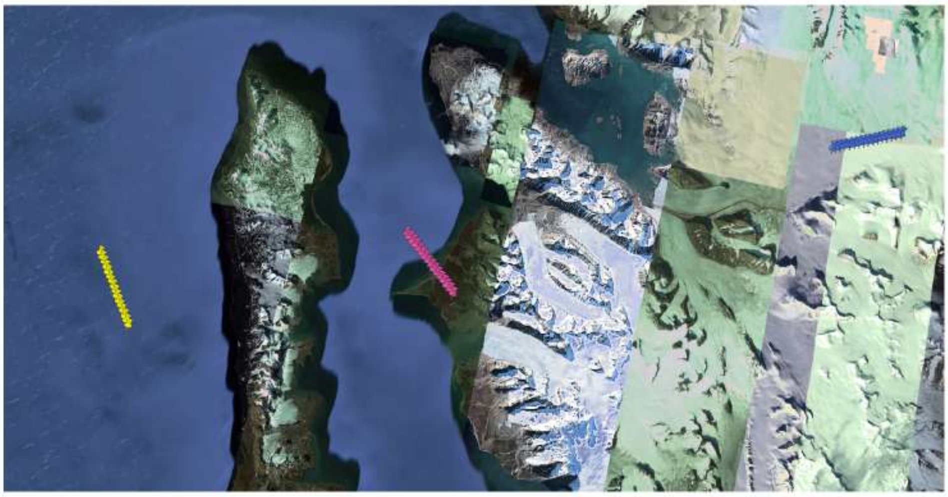

Fig. 3. The yellow points (left), red points (center), and blue points (right) respectively represent the trajectories of the specular points when passing over the sea water surface in May, sea ice surface in February, and soil surface in August, respectively.

TABLE I

SNRS IN DIFFERENT CASES. USNR AND CSNR PRESENT THE UNCORRECTED DDM SNR AND THE CORRECTED DDM SNR, RESPECTIVELY.

N_{coh}	M_{incoh}	Sea		Ice		Soil	
		uSNR(dB)	cSNR(dB)	uSNR(dB)	cSNR(dB)	uSNR(dB)	cSNR(dB)
2	100	4.24	4.66	5.97	9.79	2.17	2.17
2	300	4.82	5.14	6.67	9.72	2.31	2.40
2	500	4.59	4.94	7.30	9.83	2.41	2.47
3	100	3.99	4.45	5.72	7.97	2.63	2.69
3	300	4.59	5.02	5.52	8.57	2.48	2.50
3	500	4.63	5.00	5.55	8.59	2.98	3.11

the corrected SNRs are higher than uncorrected SNRs in all cases. Among them, the sea, ice and soil surfaces showed an average increase in SNR of 0.39 dB, 2.95 dB and 0.07 dB, respectively.These results demonstrate the potential of the navigation bit correcting method, as it allows to increase easily the SNR, without need to increase the antenna directivity.

5. CONCLUSION

This study utilized three segments of raw data from the FY-3E satellite's GNOS-II payload in 2022. Over three different reflecting surfaces in the Spitsbergen region (approximately 78.9 N; 11.9 E): ocean surface, sea ice, and soil. A method for correcting the GPS navigation bit effect has been proposed and implemented, effectively improving the SNR of the DDMs, especially for sea ice DDMs, when the coherent time exceeds 1 ms. On average, after navigation bit correction, the SNR of sea surface DDMs, sea ice surface DDMs and soil surface DDMs increased from ~0.4 to ~3 dB, depending on the target. The results imply that DDMs obtained through this method have higher SNR without increasing the antenna size, laying a crucial foundation for further research and utilization of FY-3E raw data. Future work should consider the impact of signal incidence angle on DDM and further expand the quantity of utilized data to obtain more reliable and representative results.

6. ACKNOWLEDGMENTS

The authors would like to acknowledge the National Satellite Meteorological Center, China Meteorological Administration for providing the FY-3E/GNOS-II data. This research has also been partially funded by the National Natural Science Foundation of China under Grants 42174022 (PI: Prof. Kegen Yu); the Fundamental Research Funds for the Central Universities 2023XSCX047, Postgraduate Research & Practice Innovation Program of Jiangsu Province KYCX23_2752, Graduate Innovation Program of China University of Mining and Technology 2023WLKXJ165 (Author: Changyang Wang); the project "GENESIS: GNSS Environmental and Societal Missions – Subproject UPC", Grant PID2021-126436OB-C21 funded by the Ministerio de Ciencia e Investigación (MCIN)/Agencia Estatal de Investigación (AEI)/10.13039/501100011033 and EU EDRF "A way to make Europe".

11. REFERENCES

[1] K. Yu, *Theoretical Fundamentals of GNSS Reflectometry in Theory and Practice of GNSS Reflectometry*, Elsevier, Xuzhou, Jiangsu Province, China, 2021, doi: 10.1007/978-981-16-0411-9_4.

[2] C. Wang, et al., "Significant Wave Height Retrieval Based on Multivariable Regression Models Developed With CYGNSS Data," *IEEE Trans. Geosci. Remote Sens.*, vol. 61, pp. 1-15, 2023, doi: 10.1109/TGRS.2022.3233102.

[3] A. Alonso-Arroyo, et al., "Sea Ice Detection Using U.K. TDS-1 GNSS-R Data," *IEEE Trans. Geosci. Remote Sens.*, vol. 55, no. 9, pp. 4989-5001, 2017, doi: 10.1109/TGRS.2017.2699122.

[4] A Camps, et al., "Sensitivity of GNSS-R spaceborne observations to soil moisture and vegetation," IEEE J. Sel. Topics Appl. Earth Observ. *Remote Sens.*, vol. 9, no. 10, pp. 4730-4742, Oct. 2016, doi: 10.1109/JSTARS.2016.2588467.

[5] S. Zhang, et al., "Using CYGNSS Data to Map Flood Inundation during the 2021 Extreme Precipitation in Henan Province, China," *Remote Sens.*, vol. 13, no. 24, pp. 5181, 2021, doi: 10.3390/rs13245181.

[6] J. Xia, et al., "Calibration and Wind Speed Retrieval for the Fengyun-3 E Meteorological Satellite GNSS-R Mission", *2021 IEEE Specialist Meeting on Reflectometry using GNSS and other Signals of Opportunity (GNSS+R).*, pp. 1-4, 2021. doi: 10.1109/GNSSR53802.2021.9617699

[7] E. Valencia, et al., "Advanced architectures for real-time Delay-Doppler Map GNSS-reflectometers: The GPS reflectometer instrument for PAU (griPAU)," *Adv. Space Res.*, vol. 46, no. 2, pp. 196-207, 2010, doi: 10.1016/j.asr.2010.02.002.

[8] E. Valencia, et al., "Experimental Determination of the Sea Correlation Time Using GNSS-R Coherent Data," *IEEE Geosci. Remote Sens. Lett.*, vol. 7, no. 4, pp. 675-679, 2010, doi: 10.1109/LGRS.2010.2046135.

[9] F. Martin, et al., "Mitigation of Direct Signal Cross-Talk and Study of the Coherent Component in GNSS-R," *IEEE Geosci. Remote Sens. Lett.*, vol. 12, no. 2, pp. 279-283, 2015, doi: 10.1109/LGRS.2014.2335772.